Molecular Therapy
Nucleic Acids
Original Article

Direct delivery of Cas9 or base editor protein and guide RNA complex enables genome editing in the retina

Juliette Pulman,[1,6] Catherine Botto,[1,6] Hugo Malki,[1] Duohao Ren,[1,2] Paul Oudin,[1] Anne De Cian,[3] Marie As,[3] Charlotte Izabelle,[4] Bruno Saubamea,[4] Valerie Forster,[1] Stéphane Fouquet,[1] Camille Robert,[1] Céline Portal,[1] Aziz El-Amraoui,[5] Sylvain Fisson,[1,2] Jean-Paul Concordet,[3] and Deniz Dalkara[1]

[1]Sorbonne Université, INSERM, CNRS, Institut de la Vision, 17 rue Moreau, 75012 Paris, France; [2]Université Paris-Saclay, University Evry, Inserm, Genethon, Integrare Research Unit UMR_S951, 91000 Evry-Courcouronnes, France; [3]Laboratoire Structure et Instabilité des Génomes, INSERM U1154, CNRS 7196, Muséum National d'Histoire Naturelle, CP26 43 rue Cuvier 75231 Paris Cedex, France; [4]Université Paris Cité, Inserm, CNRS, P-MIM, PICMO, 75006 Paris, France; [5]Institut Pasteur, Université Paris Cité, INSERM AO06, Institut de l'Audition, Unit Progressive Sensory Disorders, Pathophysiology and Therapy, 63 rue de Charenton 75012 Paris, France

Genome editing by CRISPR-Cas holds promise for the treatment of retinal dystrophies. For therapeutic gene editing, transient delivery of CRISPR-Cas9 is preferable to viral delivery which leads to long-term expression with potential adverse consequences. Cas9 protein and its guide RNA, delivered as ribonucleoprotein (RNP) complexes, have been successfully delivered into the retinal pigment epithelium *in vivo*. However, the delivery into photoreceptors, the primary focus in retinal dystrophies, has not been achieved. Here, we investigate the feasibility of direct RNP delivery into photoreceptors and retinal pigment epithelium cells. We demonstrate that Cas9 or adenine-base editors complexed with guide RNA, can enter retinal cells without the addition of any carrier compounds. Once in the retinal cells, editing rates vary based on the efficacy of the guide RNA and the specific location edited within the genes. Cas9 RNP delivery at high concentrations, however, leads to outer retinal toxicity. This underscores the importance of improving delivery efficiency for potential therapeutic applications in the future.

INTRODUCTION

Gene supplementation has been successful for the treatment of rare inherited retinal degenerations (IRD) caused by single recessive mutations in genes small enough to be delivered via adeno-associated virus (AAV).[1–5] Allele-specific genomic ablation or gene correction using gene editing may extend these outcomes to diseases caused by dominant mutations or by mutations in large genes, which altogether affect a larger group of patients.[6] To date, the most advanced gene editing application in the eye was designed to excise a cryptic splice site in the *CEP290* gene to improve vision in patients suffering from Leber congenital amaurosis type 10 (LCA10). This strategy based on subretinal delivery of AAV encoding SaCas9 and two guide RNAs (sgRNAs) has been successful in non-human primates[7] and has served as the basis for the first clinical trial of gene editing in the eye (NCT03872479).

Regrettably, the use of viruses to deliver CRISPR-Cas9 gene editing tools raises the potential for permanent integration into the genome,[8] off-target gene disruption through long-term exposure to gene editing reagents as well as potential immune reactions to these proteins of bacterial origin.[9] In addition, the maximum 4.7 kb cargo capacity of AAV limits the use of new gene editing tools such as base and prime editors that could be used to treat up to 99.9% of IRD.[10–12]

In this context, transient delivery of Cas9 protein and its sgRNA as ribonucleoprotein (Cas9 RNP) using non-viral vectors is an attractive alternative, as rapid degradation of the nuclease might limit its off-target effects and alleviate the risk of genome integration. The first attempt to deliver Cas9 RNP in the retina employed cationic lipids and reached 22% editing efficiency in the gene encoding vascular endothelial growth factor A (*Vegfa)* within the retinal pigment epithelium (RPE). These results were obtained in an acute mouse model of age-related macular degeneration.[13] A second study showed a similar outcome in the RPE of wild-type mice, resulting in a more modest indel rate of 6%. This study targeted the same locus and isolated the RPE cells in contact with the RNP using reporter gene expression and also reported signs of toxicity at high Cas9 RNP concentrations.[14] Another study used a nanocapsule for the delivery of Cas RNP to the RPE with similar indel rates (around 5% indels in the total RPE).[15] And more recently, adenine-base editor (ABE) RNPs were delivered to the RPE using engineered virus-like particles and reached 21% correction in the RPE.[16]

Although these first results of gene editing in the RPE using Cas9 RNP are promising, so far, no study has reported Cas9 RNP-mediated gene

Received 22 July 2024; accepted 26 September 2024;
https://doi.org/10.1016/j.omtn.2024.102349.

[6]These authors contributed equally

Correspondence: Juliette Pulman, Sorbonne Université, INSERM, CNRS, Institut de la Vision, 17 rue Moreau, 75012 Paris, France.
E-mail: juliette.pulman@inserm.fr

editing in cells of the neural retina, notably in the photoreceptors. As the majority of mutated genes in IRD are expressed in photoreceptor cells, these cells are likely to be the main targets of gene editing applications in the coming years. To fill this unmet need, we investigated transient delivery of Cas9 protein and base editor as RNP complexes in the neural retina in comparison with RPE cells. We tested different categories of non-viral vectors that display different physico-chemical properties to assess their ability to complex and deliver Cas9 RNP into retinal cells. We show here that without any vector, Cas9 or base editor RNPs induce up to 10% of indels or base edits, in the photoreceptors of wild-type adult mice. The editing efficiency is dependent on the dose of RNP, the sequence of the sgRNA, and expression level of the targeted genes in a given cell type. We also show that physical barriers specific to our tissue of interest include photoreceptor outer segments and outer limiting membrane, which impede the entry of the RNPs into the neural retina. The delivery efficacy is further hampered by intracellular barriers, such as nuclear entry and the accessibility of the targeted gene within the genome once the RNP reaches the nucleus.

Altogether our work highlights the key parameters to consider in improving gene editing efficacy of Cas9 RNPs and in designing new classes of carrier compounds to bring them into retinal cells for therapeutic gene editing. Importantly, we highlight here the cell- and gene-specific features of Cas9-mediated gene editing that must be considered in the design and preclinical testing of gene editing therapeutics.

RESULTS

Ribonucleoprotein complexes—Cas9 protein and sgRNA—induce indels in the neural retina and in the RPE

Prior to *in vivo* experiments, we first examined the properties of Cas9 protein alone or complexed with its sgRNA (ribonucleoprotein [RNP] complex) using transmission electron microscopy (TEM) and dynamic light scattering (DLS). We used recombinant Cas9 from *Streptococcus pyogenes* (SpCas9; net charge +22) with two nuclear localization signals (NLS, net charge +5). The protein alone was visible using TEM, displaying a 10 nm (Figure 1A). We then complexed it with a previously described sgRNA targeting *Vegfa* gene (net charge −120).[13,14] The complexation of the SpCas9 protein with two NLS tags and the sgRNA gave rise to homogeneous RNP complexes (theoretical net charge of −88) with an average size of 17 nm (Figure 1A). These observations were confirmed by DLS showing a particle size distribution between 10 and 70 nm with a peak of ∼15 nm for the Cas9 RNP and of ∼10 nm for the Cas9 proteins without sgRNA (Figure 1B), consistent with previous reports.[17]

Next, we injected these RNPs without any carrier compounds into the subretinal space of adult wild-type mice in a dose-dependent assay (Figure 1C). Prior to injections, we confirmed that Cas9 RNPs were correctly complexed at all the doses by DLS (Figure S1). Then, after *in vivo* injection, DNA was extracted from the whole RPE and the whole neural retina of each injected eye 1 week after injection. Indels were quantified at the targeted *Vegfa* locus using next generation sequencing (NGS). A dose-dependent increase in indels was observed both in the RPE and neural retina up to 30 μM RNP, with no further improvement at higher doses (Figure 1D). Optical coherence tomography (OCT) analysis showed a dose-dependent toxicity, with increasing disorganization of the retina, a thinning of the ONL, and the presence of infiltrates (Figure 1E) at higher doses, which might explain the plateau of indels between 30 and 68 μM RNP in the neural retina. The dose of 30 μM was therefore chosen in all follow-up experiments.

Limited diffusion of Cas9 proteins into the neural retina

To understand the low activity of the Cas9 RNPs in the neural retina, we examined Cas9 distribution 3 days post-injection by 3D imaging of the whole eye. After segmentation of the neural retina, we see that Cas9 protein is still present in clusters in some areas (Figure 2A and Videos S1 and S2). We also see that, in Cas9 RNP injected eyes, some areas within the zone with the retinal detachment, are completely devoid of Cas9, suggesting that Cas9 has already been partially degraded or that cells receiving the Cas9 RNP had died (Figure 2A and Videos S1 and S2). Cas9 protein was almost completely degraded 7 days post-injection (Figure S2).

To have a better resolution of where the indels occur within the layers of the neural retina, we performed immunohistochemistry against the Cas9 protein on retinal cryosections. We observed that the majority of Cas9 proteins were not able to infiltrate into the neural retina (Figure 2B). Higher magnification images of the photoreceptor layer allowed us to identify outer segment discs and tight extracellular matrix of the outer limiting membrane as the main physical barriers limiting the diffusion of RNPs. We also observed that Cas9 RNPs were associated with disorganized photoreceptor outer segments (Figure 2C).

Cationic lipids do not improve Cas9 RNP-mediated indel rates in the retina

We next investigated if physical barriers specific to the neural retina could be bypassed using cationic lipids as suggested in prior studies.[13,18] Indeed, the global negative charge of Cas9 RNPs may not favor entry into cells.[18] To enter cells by endocytosis or direct penetration through the cell membrane after interaction with proteoglycans, positive surface charges are preferred. Based on this and previous studies in the inner ear and in the RPE,[13,18] we investigated the capacity of the commercial cationic lipids Lipofectamine 2000 or Lipofectamine RNAiMAX to deliver Cas9 RNPs to retinal cells.

Prior to injections *in vivo*, we examine complexation between Cas9 RNPs and Lipofectamine2000 using EM and DLS. Cas9 RNPs mixed with Lipofectamine 2000 gave heterogeneous assemblies of complexes, leaving either uncomplexed monomeric RNPs or resulting in complexes resembling liposomes and multilamellar lipoplexes of different sizes (Figures 3A–3H). DLS measurements confirmed heterogeneous composition of the mix with peaks corresponding to the detection of aggregates (Figures 3I and S3). Finally, after subretinal injection in wild-type mice, neither Lipofectamine 2000 nor

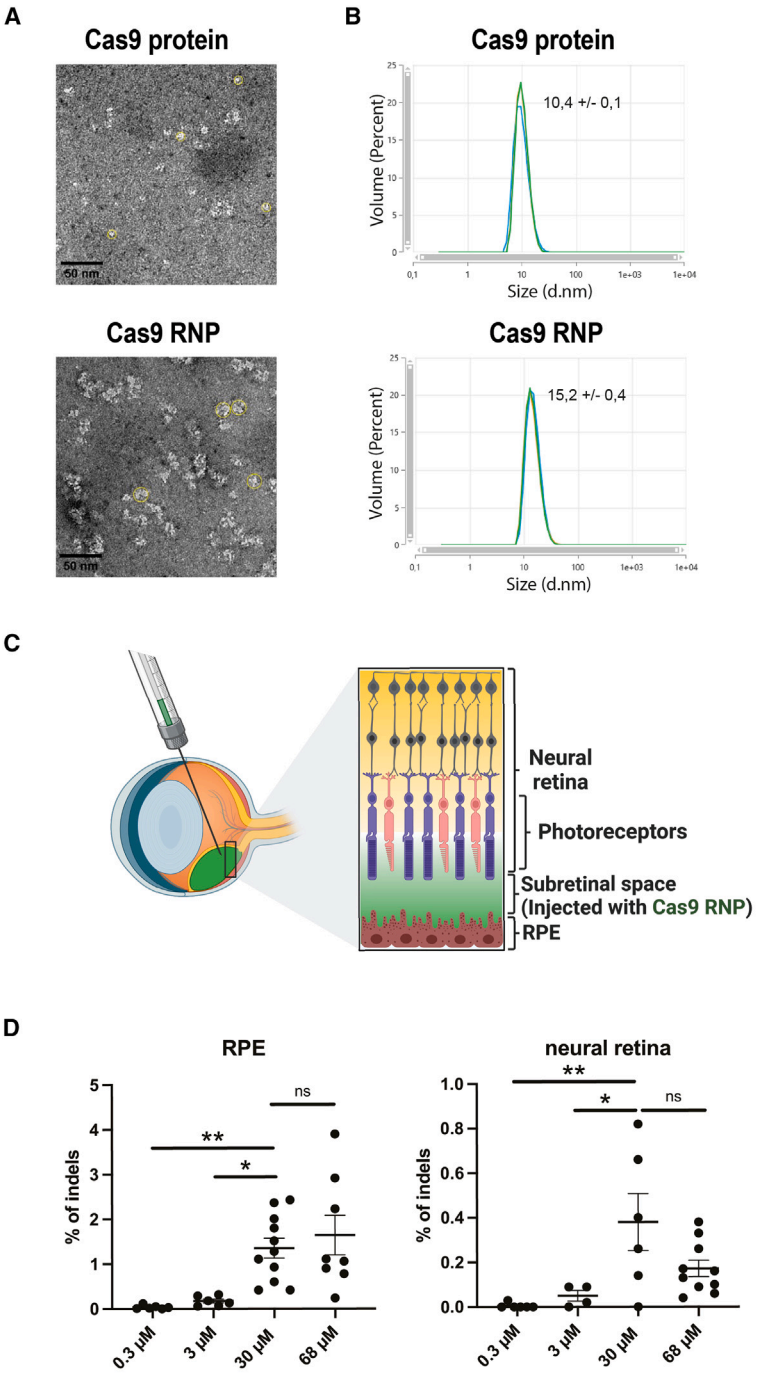

Figure 1. Direct Cas9 RNP delivery induces indels *in vivo* in the RPE and the neural retina

(A) Transmission electron microscopy (TEM) analysis of 60 μM Cas9 protein (10-nm-diameter circles are shown in yellow) and Cas9 RNP (17-nm-diameter circles are shown in yellow) imaged using 1% aqueous uranyl acetate as a negative stain. (B) Size (nm) of 30 μM Cas9 protein alone or Cas9 RNPs determined by dynamic light scattering (DLS). Three different measures (in blue, orange, and green but overlapping) were performed at 5-min intervals. Means of the peak by volume (nm) ± standard deviation. d.nm = diameter in nm. (C) Schematic representation of the subretinal injections performed in the eyes of adult wild-type mice. RPE and neural retinas are separated during dissections and analyzed independently. (D) Indels in the RPE and neural retina after subretinal injection of Cas9 RNPs at different concentrations *in vivo*. NGS analysis was performed 7 days after injection. Each dot represents RPE/neural retina isolated from a single mouse eye. Mean ± SEM. Ordinary one-way ANOVA test, Dunnett's multiple comparisons test. (E) OCT images 7 days post-injection of buffer solution, or different Cas9 RNP concentration in the injection area (temporal images) in adult wild-type mice.

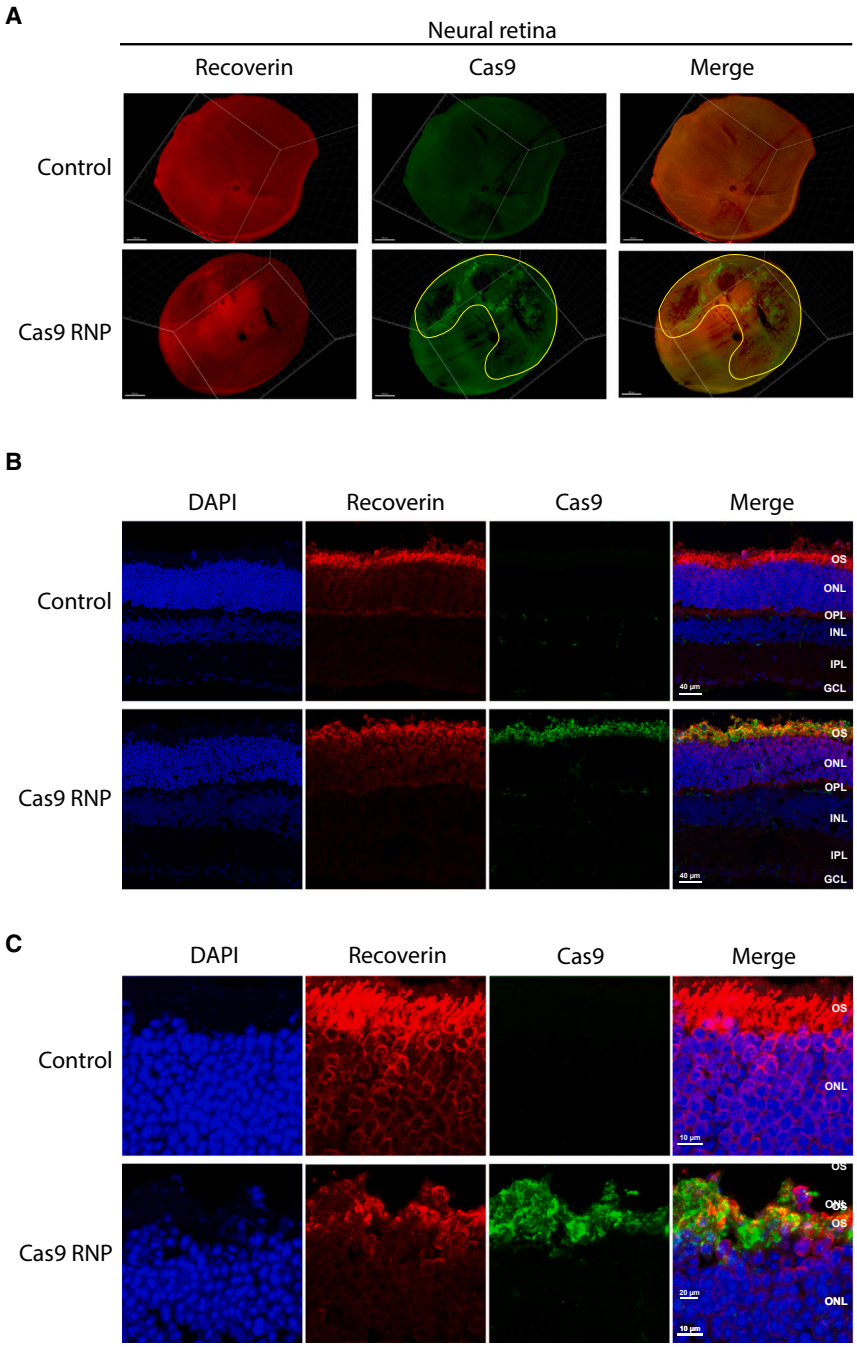

Figure 2. Localization of Cas9 protein inside the neural retina

Eyes were collected 3 days after 2 µL subretinal injection of buffer (control) or 30 µM Cas9 RNPs. (A) Top view of the entire neural retina after segmentation from mouse whole eye after clearing and 3D imaging. Injection zone area is circled in blue. Staining of the photoreceptors (Recoverin, red) and Cas9 protein (green). Scale bar, 200 µm. (B and C) Neural retina cross-sections were stained for nuclei (DAPI, blue), photoreceptors (Recoverin, red), and Cas9 protein (green). OS: outer segment, ONL: outer nuclear layer, OPL: outer plexiform layer, INL: inner nuclear layer, IPL: inner plexiform layer, GCL: ganglion cell layer. (C) Zoom on the photoreceptors outer segment and nuclei.

Lipofectamine RNAiMax improved Cas9 RNP editing in the retina (Figure 3J). Also, Cas9 complexed with Lipofectamine 2000 shows similar difficulty to Cas9 RNP to cross the ONL (Figure 3K). Moreover, cell infiltrates were observed within the disorganized OS in this region (Figure 3K).

Given the heterogeneous complexes obtained with Lipofectamine, we next evaluated a peptide-based system to improve the delivery of RNPs to the neural retina. A previous study had revealed the capacity of a shuttle peptide, named SP10, to promote complexation and delivery of Cas9 RNP into epithelial cells *in vivo*.[19] SP10 is composed of a cell-penetrating peptide (CPP) linked to an endosomolytic peptide for endosome rupture (net positive charge +10). Similar to Lipofectamine, mixing of 250 µM SP10 and 30 µM Cas9 RNPs resulted in heterogeneous complexes of 34.4 ± 3.7 nm and large aggregates (Figure S4). Switching from a lipid to a peptide thus failed to generate more homogeneous complexes with lower size distribution. The use of these complexes *in vivo* did not significantly increase the capacity of RNPs to induce indels in the retina (Figure S4).

As previous reports have shown signs of RPE toxicity after Cas9 RNP delivery with lipoplexes,[14] we also investigated the potential toxicity of naked RNP injection on the neural retina of wild-type mice by *in vivo* imaging. OCT was performed 1 month after Cas9 RNP subretinal injection and showed retinal thinning at the injection site and cellular infiltrates in eyes injected with RNP alone or RNP mixed with Lipofectamine 2000 (Figure 4A). In eyes injected with Cas9 RNP alone, retinas were less damaged than when injected with Cas9 RNP mixed with Lipofectamine 2000 (Figure 4A). We investigated if retinal disorganization in the injection zone using Cas9 RNP alone would affect the retinal function. Photopic retinal function was significantly decreased 7 days post-injection. Scotopic electroretinograms (ERGs) were lower at 1 week post-injection but the difference with the control group was not statistically significant. This tendency was still present 1 month post-injection but to a lower extent (Figure 4B). The same tendency was observed with Lipofectamine2000, both at 7 days and 1 month post-injection (Figure 4B).

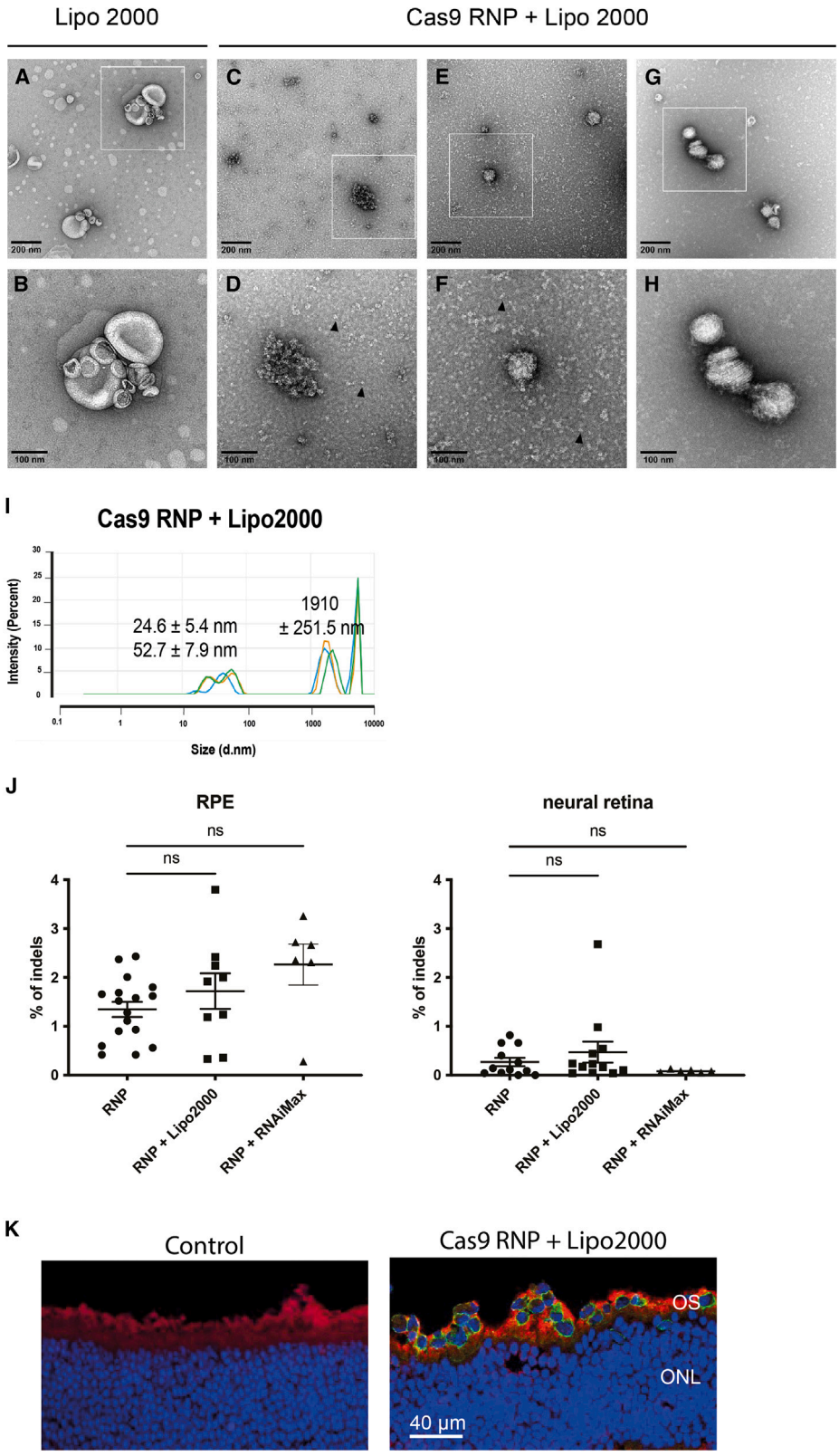

(legend on next page)

Editing efficiency depends partially on the expression level of the targeted gene but is mostly determined by the sgRNA efficiency

After investigating extracellular barriers to RNP delivery to the retina, we turned our attention to intracellular factors contributing to gene editing efficiency in retinal cells. To better understand the contribution of chromatin accessibility on editing efficiency in photoreceptors, we compared indel efficiencies obtained when targeting *Vegfa*, which is highly expressed in the RPE, or genes highly expressed in the photoreceptors (Figure S5). It is important to note that genes highly expressed in photoreceptors are often mutated in monogenic retinal diseases, and therefore constitute major targets for future therapeutic gene editing applications.[6] *Sag*, coding for S-arrestin protein; *Rho,* coding for Rhodopsin; and *Pde6b* genes were selected and sgRNAs were designed *in silico*. The efficacy of each guide was assessed in a murine cone cell line using the Tracking of Indels by Decomposition (TIDE) assay and compared with the previously tested guide targeting *Vegf*a. Among sgRNAs for the *Sag* gene, sgRNA 3 in exon 8 induced the highest rate of indels, with 24.5% of indels, which was comparable to that induced by the *Vegfa* sgRNA (Figure 5A).

Focusing on the best sgRNA targeting each of the *Sag, Rho,* and *Pde6b* genes, we further tested their efficacy *in vivo*. For genes expressed in photoreceptors, we observed an increase in the indel rates in the neural retina compared with the RPE (Figure 5B). Conversely, when targeting *Vegfa*, which is not expressed in the photoreceptors, the rate of indels was lower in the neural retina compared with the RPE (Figure 5B). These results suggest that the editing efficiency depends on the level of expression of the target genes within each cell type. As *Sag* sgRNA 3 showed a massive increase in the rate of indels (7.2% ± 3.9%) in the neural retina compared with all the others, we wondered if this was specific of the gene chromatin accessibility or of the sgRNA. We thus tested two other sgRNAs screened *in vitro* for *Sag*. Interestingly, sgRNA 1 and 2 gave very low rates of indels (Figure 5C), suggesting that the efficacy exceedingly depends on the gRNA sequence and position on the targeted gene locus. This suggests that gene editing might be more successful in certain gene targets than others. Importantly, the substantial difference in indel efficacy of *Sag* sgRNA 3 was not visible during the *in vitro* screening experiments (Figure 5A). This finding suggests that sgRNA screens conducted *in vitro* have relatively limited predictive value toward *in vivo* efficacy.

In the neural retina, we wanted to confirm that editing was mostly in the photoreceptors as they are the first to be exposed to the RNPs when injected sub-retinally. We extracted the photoreceptors from the neural retina using vibratome sectioning.[20] We confirmed that we properly extracted the photoreceptors by RNA sequencing, showing enrichment of the rods and cones in the photoreceptors extracted samples (Figure 5D). And we confirmed that the indels generated by the Cas9 RNP were located in the photoreceptors (Figure 5E).

AAV.Cas9 delivery needs a high dose to be as efficient as Cas9 RNP and generates off-target events

Our results show, for the first time, that Cas9 RNPs can efficiently edit photoreceptors when combined with an sgRNA targeting a transcriptionally active locus with an efficient guide RNA. At this stage, we wanted to compare the efficacy of "naked" RNP delivery with the state-of-the-art method of gene editing in the photoreceptors; namely, AAV vectors encoding Cas9 and sgRNA.[6] We produced two AAVs, one containing SpCas9 and one containing our *Sag* sgRNA 3 according to Wu et al.[21] The two AAVs were mixed prior to injection and injected in a single subretinal injection. The doses shown are the total of the two AAVs. We confirmed a dose-dependent expression of the SpCas9 and of the sgRNA (Figures 6A and 6B). We then measured the editing using NGS sequencing. At a usual dose of 1×10^{10} vg/mL (= 1×10^{13} vg/μL), we obtained only 1.5% ± 0.1% indels in the whole neural retina (Figure 6C). It requires a very high dose of 2×10^{11} vg/mL, known to be toxic,[22] to obtain indels similar to Cas9 RNP (Figure 6C). We also compared the editing of the five most probable off-targets of sgRNA 3 defined by COSMID (https://crispr.bme.gatech.edu/) with AAV or RNP delivery (Figure 6D). Editing in off-target 1 was more abundant in AAV than RNP. No significant edition was found in the other off-targets (Figure 6E). This suggests that Cas9 RNPs are competitive in terms of on-targets compared with the current standard AAV injection and might be safer for off-targets.

Base editor RNPs generate efficient gene editing in the retina

One significant advantage of direct RNP delivery over AAV-mediated delivery of Cas9 and sgRNA is that theoretically there is no size limit for this mode of delivery: nucleases, base editors, transposases/recombinases, and prime editors can all be delivered without any carrier vector, only complexed with their sgRNA. To prove this point and to test under identical conditions the efficacy of base editing compared with Cas9, we evaluated the editing efficacy of naked base editor RNPs complexed to the *Sag* sgRNA 3.

Both ABE protein alone and ABE RNPs gave heterogeneous mixes, as shown by TEM and by the high polydispersity index of the DLS

Figure 3. RNP delivery to the retina using cationic lipids: heterogeneous assemblies of complexes and no efficacy improvement

(A–H) TEM analysis of (A and B) Lipofectamine 2000 undiluted and (C–H) different complexes observed when mixing Cas9 RNP and Lipofectamine 2000 (diluted 100×). Monomers of RNP (D and F) are highlighted with black arrows. (I) Size of 30 μM Cas9 RNP complexed with Lipofectamine 2000 determined by DLS. Three different measures (in blue, orange, and green) were performed at 5-min intervals. Means of the peak by intensity (nm) ± standard deviation. d.nm = diameter in nm. (J) Indels induced in the whole RPE and neural retina after 2 μL of subretinal injection of 30 μM Cas9 RNPs complexed with cationic lipids: Lipofectamine 2000 or RNAiMAX *in vivo* in wild-type (WT) mice. NGS analysis was performed 7 days post-injection. Each dot represents RPE/neural retina isolated from a single mouse eye. Mean ± SEM. Ordinary one-way ANOVA test, Dunnett's multiple comparisons test. (K) Neural retina cross-sections were stained for nuclei (DAPI, blue), photoreceptors (Recoverin, red) and Cas9 protein (green). OS: outer segment, ONL: outer nuclear layer.

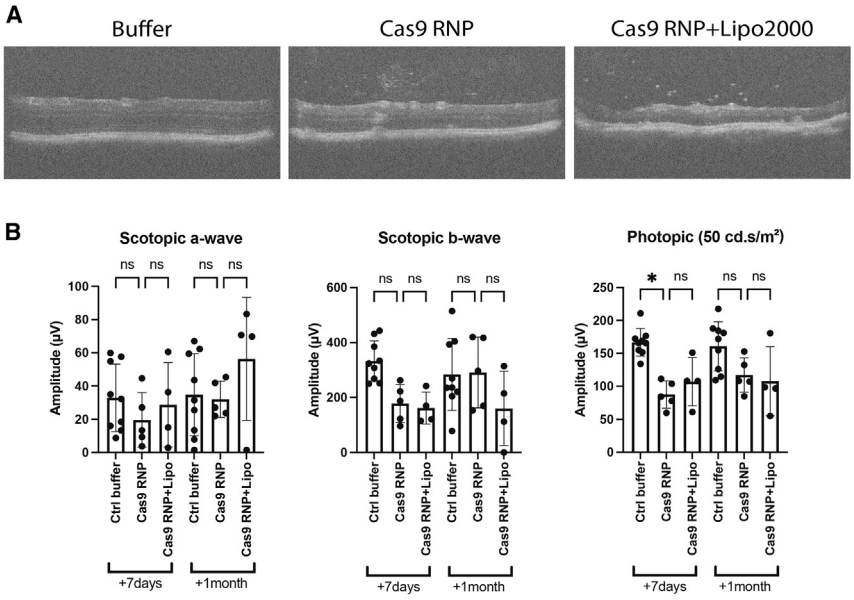

Figure 4. Functional consequences of the RNP delivery and toxicity

(A) OCT images 1-month post-injection of buffer solution in the bleb area (dorso-temporal injections), 30 μM Cas9 RNPs or Cas9 RNPs complexed with Lipofectamine 2000 in adult wild-type (WT) mice. (B) ERG analysis of control buffer vs. 30 μM Cas9 RNPs naked in adult WT mice. Only amplitudes for the highest light stimulations are represented (20 cd s/m^2 candela per square meter) for scotopic and 50 cd s/m^2 for photopic).

measurement (Figures 7A and 7B). Especially in the ABE RNPs, some aggregates from a few hundred to a few thousand nm were observed in TEM. But, for both conditions, most of the particles were between 20 and 30 nm in TEM (Figure 7A). Those results were confirmed by DLS (Figure 7B). Three days after subretinal injection, the base editor RNPs showed a similar distribution across the neural retina than Cas9 RNP, with most of it being retained in the outer segments and a toxic effect with cell infiltrates in the outer segments (Figure 7C). We also analyzed, using NGS sequencing, the % of targeted substitution and of bystanders (Figure 7D). Base editor RNPs also showed a similar editing efficacy to Cas9 RNP, yielding 10.7% ± 4.4% of targeted base changes (Figure 7E), along with 0.2% of bystander effects and no detectable indels. We confirmed the presence of the targeted substitution in the mRNA with correlations with the substitution rate found at the DNA level (Figure 7F). This confirms that the substitution was present in the photoreceptors, expressing the *Sag* gene.

Our results collectively show that RNP delivery is feasible across different editing tools and that robust outcomes can be obtained in terms of gene editing efficacy when targeting the same locus. This result further shows that RNP delivery can be an advantageous mechanism to perform side-by-side comparisons of genome editing reagents.

DISCUSSION

Regardless of the gene's size and nature of the disease-causing mutation, gene editing tools provide unprecedented opportunities for effective and long-lasting treatment of both dominant and recessive forms of genetic blindness.[10,23] In this context, persistent expression of the gene editing proteins is undesirable and there is high interest in developing a transient delivery system for their safe use in gene therapy. To this aim, we investigated the potential of direct delivery of Cas9 and its sgRNA into retinal cells with a particular focus on the photoreceptors *in vivo*. We showed that Cas9 RNPs, injected into the subretinal space without any carrier compounds generated around 10% of indels on the *Sag* gene in the photoreceptors of adult wild-type mice. To our knowledge, this is the first report of an editing efficiency for a Cas9 RNP molecule delivered without any vectors in the RPE and the photoreceptors. Although the percentage of gene edition needed for a therapeutic effect will highly depend on the disease-causing gene, pathogenic mechanisms and kinetics, 15% efficacy might have therapeutic relevance (e.g., Maeder and colleagues estimated that an editing efficacy of 10% may provide measurable benefit to LCA10 patients affected by mutations in *CEP290*).[7]

Until now, gene editing RNPs delivered using a variety of vectors have shown efficiency in the RPE only and there have been no reports of RNP efficacy in the photoreceptors.[24] Using Cas9 RNPs, the gene editing efficacy in the RPE varied between 6% and 24% within the injected area following subretinal delivery using cationic lipids[13,14] and it reached 17% using lentivirus-derived nanoparticles.[24] In our case, instead of analyzing indel rates in the injected area (covering approximately half of the retinal surface), we measured the indel rates of the entire RPE and neural retina. Under these conditions, we achieved 10% of indels in the photoreceptors and 2% in the RPE. Our editing rates in the RPE are close to previous reports[13,14] if we extrapolate to the whole retina. Remarkably, we show for the first time that gene editing RNPs without any vector system can edit the photoreceptors at significant rates.

Thus far, the state of the art for gene editing in the neural retina has been AAV vectors encoding Cas9 and sgRNAs.[6] For example, Wu et al. used a dual AAV8 vector with saCas9 and a double sgRNA achieving 17.8% of indels in the whole neural retina.[21] Editing efficiency of our Cas9 RNP is lower compared with this study but this observed difference could be due to the use of different models, differences in sgRNA efficacy, and the use of two guide RNAs instead of one used in this study. Conversely, when we tested an AAV strategy using our selected sgRNA 3 in wild-type mice, the dose of AAV necessary to obtain around the same editing efficiency as Cas9 RNP delivery was very high and known to be toxic.[22] We also noticed that the sgRNA seems to be the limiting factor for AAV delivery.

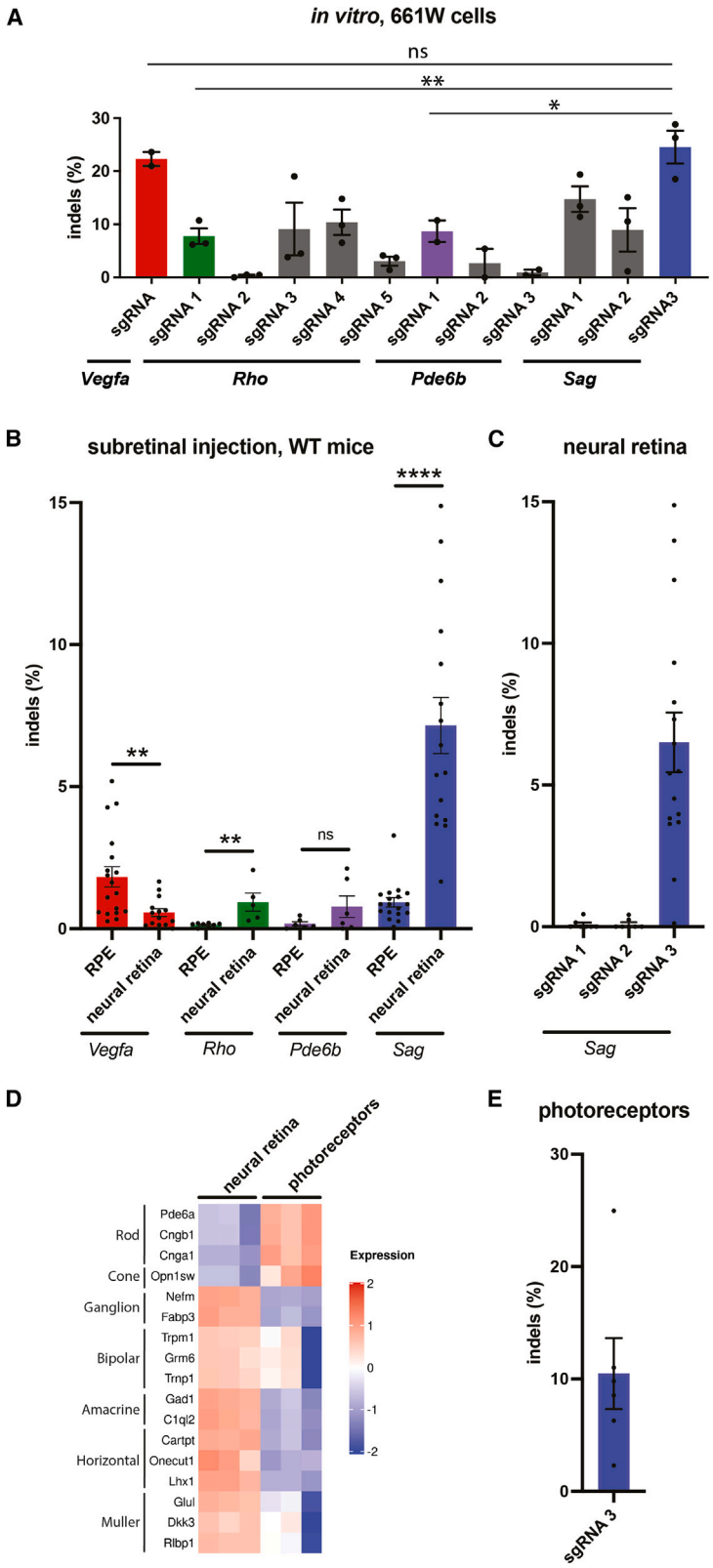

Figure 5. Efficiency of different sgRNAs targeting genes highly expressed in the retina

(A) Validation of sgRNAs targeting genes highly expressed in photoreceptors (*Sag*, *Rho*, and *Pde6b*), compared with the sgRNA targeting *Vegfa* gene by TIDE assay. Transfection of Cas9 RNPs complexed with Lipofectamine 2000 in 661W cell line. Mean ± SEM. Ordinary one-way ANOVA test, Dunnett's multiple comparisons test. sgRNAs that were selected for further *in vivo* studies are highlighted in colors. (B) Frequencies of indels induced in the whole RPE and whole neural retina of wild-type (WT) mice after subretinal injection of 30 μM Cas9 RNPs with *Sag* sgRNA 3; *Rho* sgRNA1 or *Pde6b* sgRNA1 and compared with the *Vegfa* sgRNA. NGS analysis was performed 7 days post-injection. Each dot represents RPE/neural retina isolated from a single mouse eye. Mean ± SEM. Ordinary one-way ANOVA test, Dunnett's multiple comparisons test. (C) Frequencies of indels induced in the whole neural retina of WT mice after subretinal injection of 30 μM Cas9 RNPs with *Sag* sgRNA1; *Sag* sgRNA2 or *Sag* sgRNA 3. NGS analysis was performed 7 days post-injection. Each dot represents neural retina isolated from a single mouse eye. Mean ± SEM. (D) Heatmap representation of the log2 VST DESeq2 values for the main retinal cell types in three samples in which the whole neural retina was extracted and the three samples in which the photoreceptors were extracted using vibratome. (E) Frequencies of indels induced in the photoreceptors of WT mice after subretinal injection of 30 μM Cas9 RNPs with *Sag* sgRNA 3. NGS analysis was performed 7 days post-injection. Each dot represents photoreceptors isolated from a single mouse eye. Mean ± SEM.

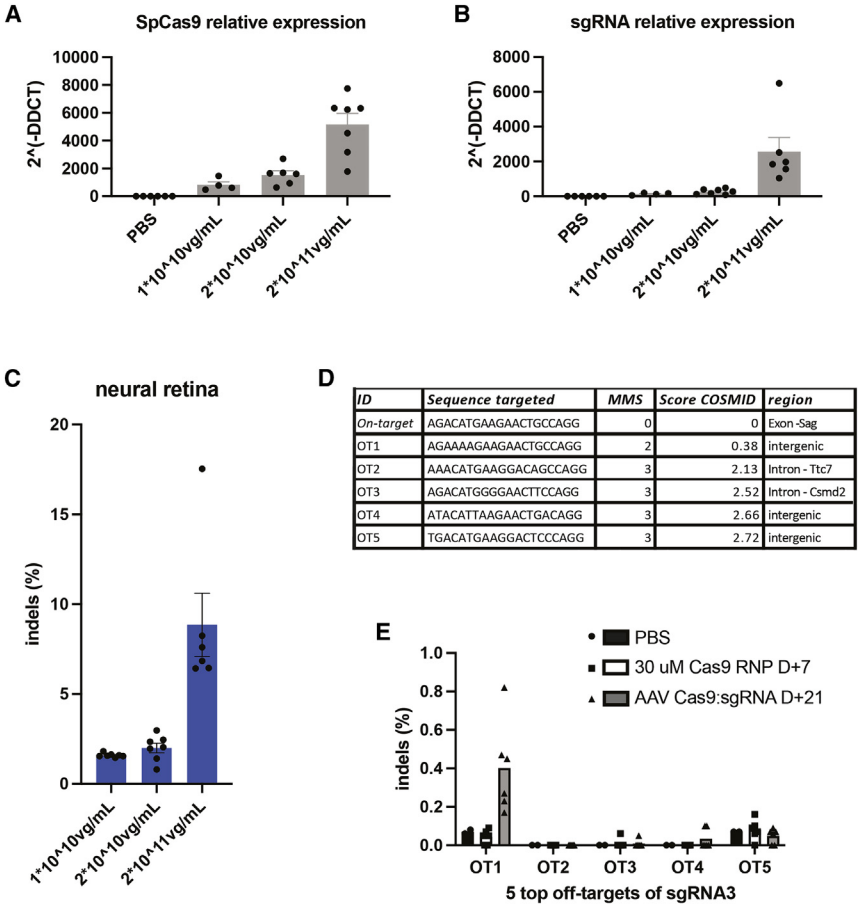

ID	Sequence targeted	MMS	Score COSMID	region
On-target	AGACATGAAGAACTGCCAGG	0	0	Exon -Sag
OT1	AGAAAAGAAGAACTGCCAGG	2	0.38	intergenic
OT2	AAACATGAAGGACAGCCAGG	3	2.13	Intron - Ttc7
OT3	AGACATGGGGAACTTCCAGG	3	2.52	Intron - Csmd2
OT4	ATACATTAAGAACTGACAGG	3	2.66	intergenic
OT5	TGACATGAAGGACTCCCAGG	3	2.72	intergenic

Figure 6. AAV.Cas9 delivery: efficacy and genomic safety

(A and B) Relative expression of SpCas9 (A) and sgRNA 3 (B) 21 days after subretinal injection of AAV.SpCas9 and AAV.sgRNA 3. Results of qPCR after 2^(-ddCT) analysis using β-actin as a reference gene. Mean ± SEM. (C) Indels in the neural retina after subretinal injection of three different doses of AAV.Cas9 and AAV.sgRNA 3. NGS analysis was performed 21 days after injection. Each dot represents a neural retina isolated from a single mouse eye. Mean ± SEM. (D) Table of the five top off-targets of sgRNA 3 according to COSMID (https://crispr.bme.gatech.edu/). MMS: number of mismatches. (E) Indels of the five top off-targets of sgRNA3 in the neural retina. For AAV delivery, the highest dose of 2×10^{11} vg/mL (total) was used. For the RNP delivery, the optimized 30 μM Cas9 RNP was used. NGS analysis was performed 7 days after injection for the RNP and 21 days after injection for the PBS and the AAV. Each dot represents a neural retina isolated from a single mouse eye. Mean ± SEM.

Optimization of the ratio of sgRNA and Cas9 might improve its efficacy. Moreover, we found off-target events when using AAV that was not present when using Cas9 RNP. This comparison should be taken with caution because of differences in the dose, the quantity, and kinetics of the two delivery methods and we have spent significantly more effort toward optimizing the RNP delivery parameters as compared with AAV.

As for base editing, BEs have been delivered by subretinal injection via dual AAVs into photoreceptor cells, resulting in 21%–26% editing of the photoreceptor cells.[25,26] BEs were also delivered using a single lentiviral vector system into the RPE, resulting in around 16% editing rate[27] whereas BEs delivered as RNPs complexed with Lipofectamine 2000 achieved only 2% efficiency in the same cells.[28] In our work, naked RNPs were able to yield up to five times more base editing in the whole neural retina. However, gene editing in the retina using RNP is still only half as efficient as that obtained using AAVs.

The use of non-viral vectors is likely necessary to improve the delivery efficacy and lower the dose-related toxicity of RNPs for therapeutic gene editing in the retina. Cationic lipids such as Lipofectamine 2000 or peptide-based carriers used in this work did not improve the editing efficiency and were toxic to the retina suggesting other types of vectors or conjugates must be optimized toward delivery into retinal cells. Such vectors may also shield RNPs from immune cells improving their overall safety.

We demonstrated that following RNP injections into the subretinal space, the majority of Cas9 proteins accumulate over the neural retina and seem unable to infiltrate the dense OS structures and extracellular matrix of the outer nuclear layer. Photoreceptors form a dense layer of cells that present specific barriers such as photoreceptor outer segments and the external limiting membrane posing a physical size limit to the particles that are injected into the retina from the subretinal route. In the case of RNP delivery, it remains to be determined if the breakdown of the external limiting membrane was an initial event of the RNP injection.

Targeting elements increasing the capacity of the complexes to bind and enter photoreceptor cells will be crucial to increase delivery efficacy.[15,29] Attempts to decorate RNP nanocarriers with molecules, such as all-*trans* retinoic acid, have been successful to increase entry into the RPE. But, so far, there is no report of compounds increasing the targeting of RNPs to photoreceptors.[15] However, such compounds are being tested for mRNA delivery and may prove useful in decorating RNPs. In a recent study, lipid nanoparticles decorated with peptides for Cas9 mRNA delivery generated 0.5% indels in the whole RPE and no gene editing in the photoreceptors,[30] highlighting the difficulty of the transient delivery of CRISPR-Cas9 to the retina, whether in form of mRNA or RNP. This study also highlighted the significant gap between the delivery of reporter gene mRNA and of mRNA encoding a gene editing tool, with the latter being significantly more challenging. Even though transient delivery of CRISPR-Cas9 holds great promise for reducing the risks of off-target, bystander effect, and immune response;

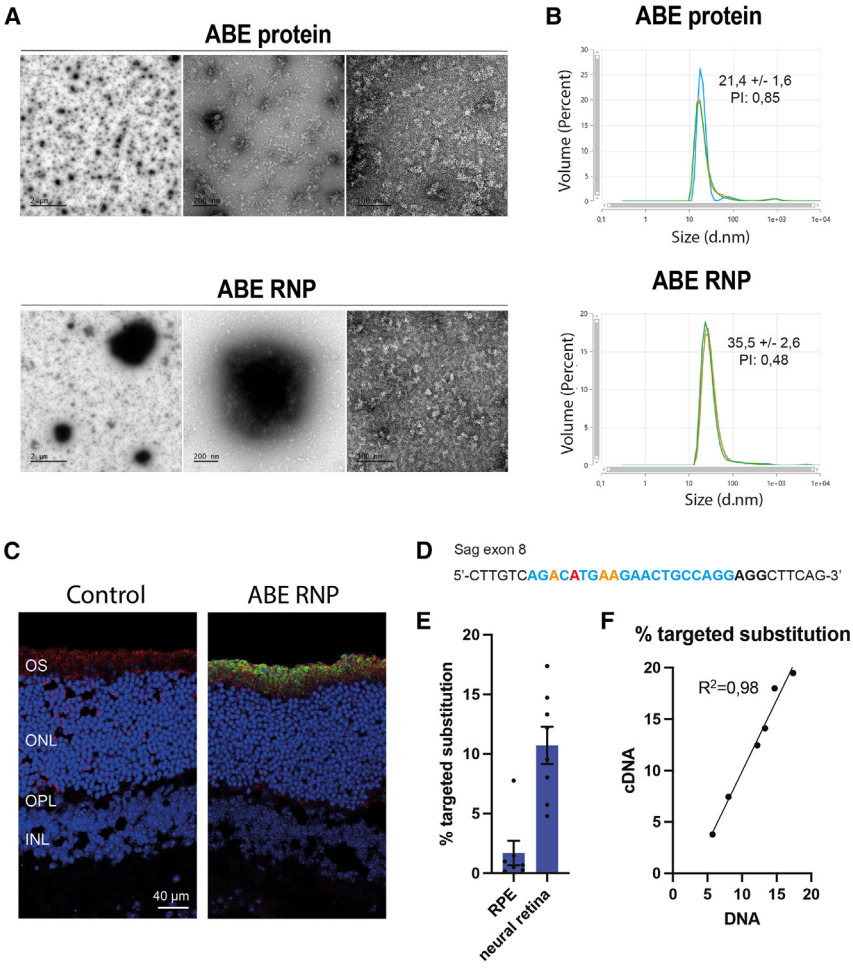

Figure 7. ABE RNP delivery to the retina is able to generate targeted substitution

(A) Transmission electron microscopy (TEM) analysis of 30 µM ABE protein and ABE RNP imaged using 1% aqueous uranyl acetate as a negative stain. For the picture of ABE RNP at 200 nm, the Gamma was manually adjusted in order to see details within the protein aggregate. (B) Size of 30 µM ABE protein alone or ABE RNP determined by DLS. Means of the peak by volume (nm) ± standard deviation. PI: polydispesity index. (C) Neural retina cross-sections were stained for nuclei (DAPI, blue), photoreceptors (Recoverin, red), and ABE (SpCas9 protein, green). OS: outer segment, ONL: outer nuclear layer, OPL: outer plexiform layer, INL: inner nuclear layer. (D) Schematic of the base editing strategy. In black bold, the PAM; in blue, the spacer; in red, the targeted nucleotide; and in orange, the bystanders. (E) Frequencies of on-site substitutions in the RPE and the whole neural retina of WT mice after subretinal injection of 30 µM ABE RNPs with Sag sgRNA 3. NGS analysis was performed 7 days post-injection. Each dot represents RPE/neural retina isolated from a single mouse eye. Mean ± SEM. Student's t test. (F) Correlation between the targeted substitution found at the DNA level and at the cDNA level by NGS sequencing performed 7 days post-injection.

DNA repair pathway. Heterochromatin, on the other hand, influences the kinetics of Cas9 editing,[33] mostly due to inhibitory impact of nucleosomes on Cas9 binding and cleavage.[34,35] Further research is also needed to comprehensively understand the variations in gene editing efficacy across different cell types of the retina, especially *in vivo*.

significant efforts will be necessary to improve the currently low efficacy in the photoreceptors as compared to AAV delivery.

Once infiltration across the extracellular physical barriers and intracellular entry is obtained, it is also of great interest to increase the endosomal escape capacity of RNPs as only the complexes that escape ubiquitination and degradation have a chance to reach the nucleus.[31] Nuclear entry can be improved to increase success rates of gene editing using RNPs. Addition of NLS sequences has previously been explored toward this aim showing that only a small number of NLS are beneficial as too many NLS sequences sterically hinder binding to the target DNA locus.[32]

Then, as RNP complexes reach the nucleus, the role of the sgRNA seems to be the most important parameter determining gene editing rates. We demonstrate that the sgRNA efficacy varies depending on the cell type and the level of expression of the targeted gene. Indeed, our editing rates were higher when targeting photoreceptor expressed genes in photoreceptors and conversely in the RPE. Indeed, the state of chromatin in eukaryotes exerts a profound influence on various stages of genome editing: Cas9 binding and cleavage, and choice of

However, we showed that efficiency mostly depends on the sgRNA sequence and the position on the targeted gene locus. The sgRNA for a specific experiment is currently chosen by applying design tools that predict the most active and efficient guides using machine learning but these tools do not take into account cell-type-specific features such as chromatin accessibility and cell cycle state of the cell. The computational scoring methods place emphasis on minimizing off-target binding by minimizing mismatches with the target sequence. Other parameters of the sgRNA, such as the GC content, affect its stability and therefore the editing efficiency. Selecting the right design tool, and experimental workflow and achieving a successful gene editing experiment is now possible for *in vitro* applications. But *in vivo* gene editing is tissue and cell-type specific, requiring additional experiments to perform relevant optimization.

In conclusion, our work shows the possibility to transiently deliver Cas9 or base editors directly as an RNP into the RPE and the photoreceptors *in vivo* and identifies the set of parameters for optimization of RNP delivery strategies into these tissues. As RNP delivery is feasible across different proteins, with similar results between Cas9

and adenine-base editors, it can be of use for quick side-by-side comparisons of new gene editing tools.

MATERIALS AND METHODS

sgRNA design

sgRNAs targeting mouse *Pde6b*, *Sag*, and *Rho* genes were designed using CRISPOR outside of nucleosome regions predicted with previously published tools.[36,37] The sgRNA targeting the vascular endothelial growth factor A (*Vegfa*) gene was published by Kim and colleagues.[13] All sgRNAs were synthesized and purified using the GeneArt Precision gRNA Synthesis Kit (Invitrogen), according to the manufacturer's protocol. sgRNAs eluted in water were aliquoted and stored at −80°C. All 20 pb sequences targeted by each sgRNA are listed in Table S2.

Cas9 nuclease

For *in vivo* experiments, *Streptococcus pyogenes* Cas9 (SpCas9) nuclease with two nuclear localization sequences (NLS) (one on its N and one on its C terminal) was produced as previously described in Menoret et al.[38] and kept at −80°C until use. For *in vitro* experiments, SpCas9 nuclease (Aldevron) was aliquoted and kept at −20°C until use. Plasmid for *E. coli* expression of ABE (Addgene #161788 from the Liu lab) was modified to express the ABE variant ABE8-13m[39] and ABE8-13m purification was performed as recommended in Huang et al.[40]

RNP preparation and complexation

Ribonucleoproteins (RNPs) were prepared immediately before use. Briefly, SpCas9 proteins were mixed to sgRNAs at a molar ratio Cas9 protein/sgRNA of 1:1 in a final buffer concentration of 20 mM HEPES/200 mM KCL (pH7.4). SpCas9/sgRNA solution was incubated at room temperature for 5 min before direct use or complexation with a vector. Freshly prepared RNPs were mixed with several non-viral vectors, then solutions were vortexed for 10 s and incubated at room temperature for 10 min before direct use. Lipofectamine 2000 and Lipofectamine RNAiMAX Transfection Reagent (Invitrogen) were purchased from Thermo Fisher. Shuttle peptides were synthetized by Covalab.

AAV production

Plasmids were constructed according to Wu et al.[21] The AAV.SpCas9 was constructed exactly as Wu et al. with an sCMV promotor. And for the AAV.sgRNA 3, we replaced sgA with our *Sag* sgRNA 3 and removed sgB. We replaced the additional replacement containing cmh-RHO with a CAG>EGFP marker. We bought the plasmids at VectorBuilder.

AAV8 vectors were produced as previously described using the co-transfection method and purified by iodixanol gradient ultracentrifugation.[41] AAV vector stocks were titered by quantitative polymerase chain reaction (qPCR)[42] using SYBR Green (Thermo Fisher Scientific).

Transmission electron microscopy

Samples were prepared following the negative staining protocol reported by Rames et al.[43] Briefly, a glow discharged Carbon/Formvar grid (Agar Scientific, Stansted, United Kingdom) was inverted onto a 5 µL drop of the sample. After 1 min, the grid was blotted with filter paper and rinsed by quickly touching a drop of water and blotting (three times). The grid was then floated consecutively on three drops of 1% aqueous uranyl acetate for 10 s, 10 s, and 1 min, blotted, and air dried for 20 min before observation. Images were acquired using a Jeol 1400 Flash Transmission Electron Microscope (Jeol, Croissy-sur-Seine, France) operated at 120 kV and equipped with a RIO CMOS camera (Ametek SAS, Elancourt, France).

Dynamic light scattering

The hydrodynamic diameter (size) of each complex was measured using dynamic light scattering (DLS) (Zetasizer nano analyzer ZS; Malvern Instruments) at Paris ESPCI facility or using the Stunner (Unchained Labs). Three different measures were carried out with 5 min in between each.

Cell culture and transfection

Murine cone 661W cell line (ATCC, Virginia, USA) was cultivated in Dulbecco's modified Eagle's medium (DMEM, Gibco) complemented with 10% (v/v) fetal bovine serum (FBS, Gibco) and 1% penicillin-streptomycin (Gibco). Cells were maintained in a 37°C, 5% CO_2, fully humidified incubator, and passaged twice weekly; 661 W were plated at 5×10^4 cells per well in a 48-well plate with a total volume 250 µL/well. Twenty-four hours after plating, cells (70%–90% confluency) were transfected with Lipofectamine 2000 following the manufacturer's protocol. Briefly, sgRNA and spCas9 were mixed by pipetting four times and were incubated at room temperature for 5 min. In parallel, 2 µL of Lipofectamine 2000 were added to a final volume of 25 µL of Opti-MEM Reduced Serum Medium (Thermo Fisher). Then Cas9 RNP solution was added to Opti-MEM/lipid solution, vortexed for 10 s, and incubated at room temperature for 10 min. Twenty-five microliters of complexed solution was added to each well to obtain a final RNP concentration of 100 nM in a total volume of 275 µL. Medium was changed 24 h after transfection and cells were harvested 48 h after transfection. Cell pellets were washed with PBS and frozen at −20°C until DNA extraction.

Subretinal injections in mice

All animal experiments were realized in accordance with the NIH Guide for Care and Use of Laboratory Animals (National Academies Press, 2011). The protocols were approved by the Local Animal Ethics Committees and conducted in accordance with Directive 2010/63/EU of the European Parliament. The project was evaluated by the CEEA 05 (Ethical Committee in Animal Experimentation 05) and approved by the MESRI ("ministère de l'enseignement supérieur, de la recherche et de l'innovation", France). The approval numbers of the projects from the animal facility are B-75-12-02 and C-75-12-02.

C57BL/6j wild-type mice (Janvier Laboratories) were used for this study. For ocular injections, mice were anesthetized by isoflurane inhalation. Pupils were dilated and subretinal injections (dorso-temporal injections) of 2 µL were performed using a Hamilton syringe with a 33-gauge blunt needle (World Precision Instruments, Inc.)

under an operating microscope (Leica Microsystems, Ltd.). Ophthalmic ointment (Fradexam) was applied after surgery. Eyes with extensive subretinal hemorrhage were excluded from the analysis. Animals were euthanized by CO_2 inhalation and cervical dislocation. For indels analysis, after 7 days the whole RPE and the whole neural retina were isolated without selection of transfected cells.

Samples preparation for quantification of indels

For RPE tissue or *in vitro* cells, genomic DNA was extracted using the NucleoSpin DNA tissue (Macherey-Nagel). Each experimental condition was incubated in lysis buffer and proteinase K at 56°C for 3 h for RPE tissue and 10 min for *in vitro* cells. Further steps were performed following the manufacturer's instructions.

For neural retina tissue, DNA and RNA were extracted using the Quick-DNA/RNA Microprep Plus Kit (Ozyme) according to the manufacturer's instructions.

For photoreceptor extraction, the protocol described by Clérin et al. was used[20] and then the DNA and RNA were extracted using the Quick-DNA/RNA Microprep Plus Kit (Ozyme) according to the manufacturer's intructions.

PrimeSTAR GXL DNA polymerase (Takara) was used for PCR amplification. Primers for amplifying region of interest are listed in Table S3. The thermal cycler program for PCR was as follows: 98°C for 10 s, followed by 60°C for 15 s, and finally 68°C for 20 s, with in total 30 cycles. PCR samples were then purified using NucleoSpin PCR and gel kit (Macherey-Nagel) following the manufacturer's instructions. Purified amplicons were verified by electrophoresis on a 1% agarose gel. For *in vivo* experiments, PCR amplicons were sent to next generation sequencing (NGS) at the Massachusetts General Hospital DNA core facility. A total of 10,000 reads were generated per sample and analyses were done with a cutoff of 10 reads. For *in vitro* experiments, PCR amplicons were sent to Sanger sequencing (Eurofins) and indels were analyzed using TIDE (Tracking of Indels by Decomposition) Analysis (https://tide.deskgen.com/). For the NGS sequencing, analysis was done using a reference sequence from untreated samples and setting the parameters to detect a maximum indels size of 10 nucleotides.

For measurement of the indels on the cDNA, reverse transcription reaction was conducted on the mRNA using the SuperScript IV reverse transcription kit (Invitrogen). Extracted RNA were submitted to DNAse TURBO (Invitrogen) treatment prior to reverse transcription according to the manufacturer's instructions.

qPCR analysis

Seven days post-injection, retinas were collected from each experimental condition. DNA and RNA were extracted using the Quick-DNA/RNA Microprep Plus Kit (Ozyme) according to the manufacturer's instructions. Reverse transcription (RT) was performed with Superscript Reverse Transcriptase III, following the manufacturer's instructions with oligodT primers (Thermo Fischer Scientific). For qPCR, samples were run at duplicates with no-RT controls to confirm the absence of genomic DNA. Duplicates that had a standard deviation above 0.5 were removed. Primers used are listed in Table S4. cDNA levels were determined with relative cDNA quantification and are expressed as the fold induction compared with control groups (injected with PBS).

Statistical analysis

All statistical analyses were carried out using GraphPad Prism version 7.0. p values were determined by ordinary one-way ANOVA test, Dunnett's multiple comparisons test if more than two conditions analyses or two-tailed parametric paired Student's t test for the analyses on base editors indels (two conditions compared). ns: non-significant, $^{*}p < 0.05$, $^{**}p < 0.005$, $^{***}p < 0.0005$, $^{****}p < 0.0001$.

RNA sequencing

RNA quality and quantity were evaluated using BioAnalyzer 2100 (Agilent Technologies, Santa Clara, CA) with the RNA 6000 Nano Kit (Agilent Technologies, Cat. #5067-1511). RNA sequencing libraries were constructed from 300 ng of total RNA using a modified TruSeq RNA Sample preparation kit protocol.

RNA sequencing analyses were performed as described in Couturier et al.[44] Fastq files obtained from the sequencing were aligned using STAR (v2.7.9a) against the *Mus musculus* reference genome from Ensembl, with option "–quantMode GeneCounts" to extract the raw counts for each gene, and all count files were concatenated into a single file. The count file and the sample file were loaded in our in-house R Shiny application EYE DV seq. Normalization and differential expression analysis values were computed with DESeq2 (v1.40.2).[45]

Immunostaining and imaging

One, 3, or 7 days post-injection, mouse eyes were enucleated and immediately fixed in a 4% formaldehyde solution for 1 h. Samples were either used for cryosections, flat-mount retina, or whole eye clearing and imaging.

To prepare cryosections or retinal flatmounts, eyecups were immersed in PBS-10% sucrose for 1 h and then PBS-30% sucrose overnight at 4°C. They were embedded in OCT medium and frozen in liquid nitrogen; 12-µm-thick vertical sections were cut with a Microm cryostat.

After 3 PBS washes, retinal flatmounts or cryosections were incubated in a blocking buffer for 1 h and then with primary antibodies overnight at 4°C. Primary antibodies used in this study are listed in Table S5. After three washes of the sections, the secondary antibodies (Alexa Fluor 488, 594, or 647, Thermo Fischer Scientific) were added for 2 h at room temperature, followed by three PBS washes. Retinal flatmounts or cryosections were mounted in Vectashield mounting medium (Vector Laboratories) and visualized using an Olympus confocal microscope. ImageJ software was used to process the images.

Tissue clearing and imaging

To remove pigmentation and reduce background related to hematomas, a tissue bleaching was carried out as previously described.[46] Then the EyeDISCO protocol was used to bleached and clear eye samples.[47]

For whole-mount immunostaining, samples were transferred to a solution containing the primary antibodies diluted in PBSGT and placed at 37°C with agitation for 7 days. Primary antibody dilutions are described in Table S4. After six washes of 1 h in PBSGT at RT, samples were incubated at 37°C in the secondary antibody solution for 2 days and washed six times during 1 h in PBSGT at RT.

To facilitate the handling and imaging with the light-sheet microscope, tissue samples were embedded prior to clearing in 1.5% agarose (Roth), prepared in TAE 1X (Invitrogen).

3D imaging of cleared specimens and imagine analysis

Cleared samples were imaged with a Blaze light-sheet microscope (Miltenyi Biotec) equipped with sCMOS camera 5.5MP (2560 × 2160 pixels) controlled by Imspector Pro 7.5.3 acquisition software.

To isolate the neural retina using the Imaris software, the surface tool was manually applied and the mask option was selected. Mask obtained with retina segmentation was used to highlight staining of the neural retina (using Recoverin).

SD-OCT imaging

Spectral-domain optical coherence tomography (SD-OCT) was performed 7 days or 1 month post injections. For pupil dilation, 0.5% tropicamide (Mydriaticum, Thea) and 5% phenylephrine hydrochloride (Neosynephrine, Europhta) were added to both eyes. The animals were anesthetized by inhalation of isoflurane (Isorane, Axience) and placed in front of the SD-OCT imaging device (Bioptgen 840 nm HHP; Bioptgen). The eyes were kept moist with 0.9% NaCl during the whole procedure. Images from the temporal side of the eye are shown. Image acquisitions were performed using the following parameters: rectangular scan/1000 A-scan per B-scan/100 B-scan 1 frame. ImageJ software was used to process the images as .avi.

Electroretinogram

Mice were dark adapted overnight and anesthetized by ketamine (80 mg/kg, Ketamidor, Axience)/xylazine (8 mg/kg, Rompun, Elanco). For pupil dilation, 0.5% tropicamide (Mydriaticum, Thea) and 5% phenylephrine hydrochloride (Neosynephrine, Europhta) were added to both eyes. For local corneal anesthesia, 0.4% oxybuprocaine chlorohydrate (Thea) was used and Lubrithal (Dechra) was used to maintain conductivity and corneal hydration. A reference electrode was inserted into the mouse forehead and the ground electrode was placed above the tail. Corneal lenses (Mayo Corporation, Japan) were applied on corneal surface and ColorDome D125 (Diagnosys, Lowell, MA, USA) was used for ERG recordings. Scotopic ERGs were made first using five increasing light intensity of flashes (0.001, 0.1, 1, 10, and 20 cd s/m^2) and recordings were averaged from five flashes at each light intensity. Photopic recordings were collected after adapting the mouse to a constant background light (20 cd/m^2) for 5 min and recorded at 0.1, 1, 10, and 50 cd s/m^2. Ten hertz flickers were also recorded. All data were analyzed with GraphPad Prism v.9 (GraphPad Software, La Jolla, CA, USA).

DATA AND CODE AVAILABILITY

The data that support the findings of the current study are available from the corresponding author upon reasonable request.

ACKNOWLEDGMENTS

We are grateful to S. Giovagnoli, A. Saint-Julien, Y. Rasool, L. Visticot, V. Barrios Guttierez, S. Labou, and H. Eriksson for preliminary *in vivo* and *in vitro* work, samples preparation, and indel analysis; Q. Cesar and R. Goulet (phenotypic facility) for OCT and micron recordings; and Jean Baudry for DLS access at Chimie Paris Tech.

We are grateful to the Manent family for their financial support to initiate this project and to Fondation Voir et Entendre. C.B. and J.P. were supported by grants from the Fondation pour la Recherche Médicale (FRM PLP201810007761 and SPF201909009287). This work was supported by grants from LABEX LIFESENSES [ANR-10-LABX-65], IHU FOReSIGHT (ANR-18-IAHU-01), AFM, Inserm, Sorbonne Université, Paris Ile-de-France Region (DIM Thérapie génique) and the Foundation Fighting Blindness (PPA-0922-0840-INSERM).

AUTHOR CONTRIBUTIONS

C.B., J.P., and D.D. designed experiments. A.D.C. and M.A. produced Cas9 proteins. C.B., J.P., P.O., C.I., and B.S. optimized TEM analysis. J.P. and P.O. performed and analyzed DLS recordings. C.B. designed sgRNAs and performed transfection on cell lines. C.B. and J.P. performed subretinal injections in mice. C.B., J.P., C.R., H.M., and P.O. dissected mice eyes, prepared and analyzed NGS samples. V.F. performed vibratome extraction of the photoreceptors. J.P. and D.R. performed and analyzed the RNA sequencing data. J.P. and C.B. performed histology, immunostaining, and imaging. S. Fouquet performed clearing and 3D imaging. J.P. and D.R. optimized and analyzed OCT recordings. J.P. and H.M. performed the experiments on ABE. C.P. performed and analyzed ERG recordings. C.B., J.P., and D.D. designed the study and wrote the manuscript. A.E., J.-P.C., and S. Fisson provided scientific input and gave feedback on the manuscript.

DECLARATION OF INTERESTS

D.D. is a co-inventor on patent #9193956 (Adeno-associated virus virions with variant capsid and methods of use thereof), with royalties paid to Adverum Biotechnologies and on pending patent applications on noninvasive methods to target cone photoreceptors (EP17306429.6 and EP17306430.4) licensed to Gamut Tx now SparingVision. D.D. also has personal financial interests in Tenpoint Tx. and SparingVision, outside the scope of the submitted work.

SUPPLEMENTAL INFORMATION

Supplemental information can be found online at https://doi.org/10.1016/j.omtn.2024.102349.

REFERENCES

1. Maguire, A.M., Russell, S., Chung, D.C., Yu, Z.-F., Tillman, A., Drack, A.V., Simonelli, F., Leroy, B.P., Reape, K.Z., High, K.A., and Bennett, J. (2021). Durability of Voretigene Neparvovec for Biallelic RPE65-Mediated Inherited Retinal Disease: Phase 3 Results at 3 and 4 Years. Ophthalmology *128*, 1460–1468. https://doi.org/10.1016/j.ophtha.2021.03.031.

2. Fischer, M.D., Michalakis, S., Wilhelm, B., Zobor, D., Muehlfriedel, R., Kohl, S., Weisschuh, N., Ochakovski, G.A., Klein, R., Schoen, C., et al. (2020). Safety and Vision Outcomes of Subretinal Gene Therapy Targeting Cone Photoreceptors in Achromatopsia. JAMA Ophthalmol. *138*, 1–9. https://doi.org/10.1001/jamaophthalmol.2020.1032.

3. Xue, K., Jolly, J.K., Barnard, A.R., Rudenko, A., Salvetti, A.P., Patrício, M.I., Edwards, T.L., Groppe, M., Orlans, H.O., Tolmachova, T., et al. (2018). Beneficial effects on vision in patients undergoing retinal gene therapy for choroideremia. Nat. Med. *24*, 1507–1512. https://doi.org/10.1038/s41591-018-0185-5.

4. Vignal, C., Uretsky, S., Fitoussi, S., Galy, A., Blouin, L., Girmens, J.-F., Bidot, S., Thomasson, N., Bouquet, C., Valero, S., et al. (2018). Safety of rAAV2/2-ND4 Gene Therapy for Leber Hereditary Optic Neuropathy. Ophthalmology *125*, 945–947. https://doi.org/10.1016/j.ophtha.2017.12.036.

5. Cukras, C., Wiley, H.E., Jeffrey, B.G., Sen, H.N., Turriff, A., Zeng, Y., Vijayasarathy, C., Marangoni, D., Ziccardi, L., Kjellstrom, S., et al. (2018). Retinal AAV8-RS1 Gene Therapy for X-Linked Retinoschisis: Initial Findings from a Phase I/IIa Trial by Intravitreal Delivery. Mol. Ther. *26*, 2282–2294. https://doi.org/10.1016/j.ymthe.2018.05.025.

6. Pulman, J., Sahel, J.-A., and Dalkara, D. (2022). New Editing Tools for Gene Therapy in Inherited Retinal Dystrophies. CRISPR J. *5*, 377–388. https://doi.org/10.1089/crispr.2021.0141.

7. Maeder, M.L., Stefanidakis, M., Wilson, C.J., Baral, R., Barrera, L.A., Bounoutas, G.S., Bumcrot, D., Chao, H., Ciulla, D.M., DaSilva, J.A., et al. (2019). Development of a gene-editing approach to restore vision loss in Leber congenital amaurosis type 10. Nat. Med. *25*, 229–233. https://doi.org/10.1038/s41591-018-0327-9.

8. Hanlon, K.S., Kleinstiver, B.P., Garcia, S.P., Zaborowski, M.P., Volak, A., Spirig, S.E., Muller, A., Sousa, A.A., Tsai, S.Q., Bengtsson, N.E., et al. (2019). High levels of AAV vector integration into CRISPR-induced DNA breaks. Nat. Commun. *10*, 4439. https://doi.org/10.1038/s41467-019-12449-2.

9. Charlesworth, C.T., Deshpande, P.S., Dever, D.P., Camarena, J., Lemgart, V.T., Cromer, M.K., Vakulskas, C.A., Collingwood, M.A., Zhang, L., Bode, N.M., et al. (2019). Identification of preexisting adaptive immunity to Cas9 proteins in humans. Nat. Med. *25*, 249–254. https://doi.org/10.1038/s41591-018-0326-x.

10. Anzalone, A.V., Randolph, P.B., Davis, J.R., Sousa, A.A., Koblan, L.W., Levy, J.M., Chen, P.J., Wilson, C., Newby, G.A., Raguram, A., and Liu, D.R. (2019). Search-and-replace genome editing without double-strand breaks or donor DNA. Nature *576*, 149–157. https://doi.org/10.1038/s41586-019-1711-4.

11. Gaudelli, N.M., Komor, A.C., Rees, H.A., Packer, M.S., Badran, A.H., Bryson, D.I., and Liu, D.R. (2017). Programmable base editing of A●T to G●C in genomic DNA without DNA cleavage. Nature *551*, 464–471. https://doi.org/10.1038/nature24644.

12. Komor, A.C., Kim, Y.B., Packer, M.S., Zuris, J.A., and Liu, D.R. (2016). Programmable editing of a target base in genomic DNA without double-stranded DNA cleavage. Nature *533*, 420–424. https://doi.org/10.1038/nature17946.

13. Kim, K., Park, S.W., Kim, J.H., Lee, S.H., Kim, D., Koo, T., Kim, K.-E., Kim, J.H., and Kim, J.-S. (2017). Genome surgery using Cas9 ribonucleoproteins for the treatment of age-related macular degeneration. Genome Res. *27*, 419–426. https://doi.org/10.1101/gr.219089.116.

14. Holmgaard, A.B., Askou, A.L., Jensen, E.G., Alsing, S., Bak, R.O., Mikkelsen, J.G., and Corydon, T.J. (2021). Targeted Knockout of the Vegfa Gene in the Retina by Subretinal Injection of RNP Complexes Containing Cas9 Protein and Modified sgRNAs. Mol. Ther. *29*, 191–207. https://doi.org/10.1016/j.ymthe.2020.09.032.

15. Chen, G., Abdeen, A.A., Wang, Y., Shahi, P.K., Robertson, S., Xie, R., Suzuki, M., Pattnaik, B.R., Saha, K., and Gong, S. (2019). A biodegradable nanocapsule delivers a Cas9 ribonucleoprotein complex for *in vivo* genome editing. Nat. Nanotechnol. *14*, 974–980. https://doi.org/10.1038/s41565-019-0539-2.

16. Banskota, S., Raguram, A., Suh, S., Du, S.W., Davis, J.R., Choi, E.H., Wang, X., Nielsen, S.C., Newby, G.A., Randolph, P.B., et al. (2022). Engineered virus-like particles for efficient *in vivo* delivery of therapeutic proteins. Cell *185*, 250–265.e16. https://doi.org/10.1016/j.cell.2021.12.021.

17. Nguyen, D.N., Roth, T.L., Li, P.J., Chen, P.A., Apathy, R., Mamedov, M.R., Vo, L.T., Tobin, V.R., Goodman, D., Shifrut, E., et al. (2020). Polymer-stabilized Cas9 nanoparticles and modified repair templates increase genome editing efficiency. Nat. Biotechnol. *38*, 44–49. https://doi.org/10.1038/s41587-019-0325-6.

18. Zuris, J.A., Thompson, D.B., Shu, Y., Guilinger, J.P., Bessen, J.L., Hu, J.H., Maeder, M.L., Joung, J.K., Chen, Z.-Y., and Liu, D.R. (2015). Cationic lipid-mediated delivery of proteins enables efficient protein-based genome editing *in vitro* and *in vivo*. Nat. Biotechnol. *33*, 73–80. https://doi.org/10.1038/nbt.3081.

19. Krishnamurthy, S., Wohlford-Lenane, C., Kandimalla, S., Sartre, G., Meyerholz, D.K., Théberge, V., Hallée, S., Duperré, A.-M., Del'Guidice, T., Lepetit-Stoffaes, J.-P., et al. (2019). Engineered amphiphilic peptides enable delivery of proteins and CRISPR-associated nucleases to airway epithelia. Nat. Commun. *10*, 4906. https://doi.org/10.1038/s41467-019-12922-y.

20. Clérin, E., Yang, Y., Forster, V., Fontaine, V., Sahel, J.-A., and Léveillard, T. (2014). Vibratome sectioning mouse retina to prepare photoreceptor cultures. J. Vis. Exp. 51954. https://doi.org/10.3791/51954.

21. Wu, W.-H., Tsai, Y.-T., Huang, I.-W., Cheng, C.-H., Hsu, C.-W., Cui, X., Ryu, J., Quinn, P.M.J., Caruso, S.M., Lin, C.-S., and Tsang, S.H. (2022). CRISPR genome surgery in a novel humanized model for autosomal dominant retinitis pigmentosa. Mol. Ther. *30*, 1407–1420. https://doi.org/10.1016/j.ymthe.2022.02.010.

22. Khabou, H., Cordeau, C., Pacot, L., Fisson, S., and Dalkara, D. (2018). Dosage Thresholds and Influence of Transgene Cassette in Adeno-Associated Virus-Related Toxicity. Hum. Gene Ther. *29*, 1235–1241. https://doi.org/10.1089/hum.2018.144.

23. Saha, K., Sontheimer, E.J., Brooks, P.J., Dwinell, M.R., Gersbach, C.A., Liu, D.R., Murray, S.A., Tsai, S.Q., Wilson, R.C., Anderson, D.G., et al. (2021). The NIH Somatic Cell Genome Editing program. Nature *592*, 195–204. https://doi.org/10.1038/s41586-021-03191-1.

24. Haldrup, J., Andersen, S., Labial, A.R.L., Wolff, J.H., Frandsen, F.P., Skov, T.W., Rovsing, A.B., Nielsen, I., Jakobsen, T.S., Askou, A.L., et al. (2023). Engineered lentivirus-derived nanoparticles (LVNPs) for delivery of CRISPR/Cas ribonucleoprotein complexes supporting base editing, prime editing and *in vivo* gene modification. Nucleic Acids Res. *51*, 10059–10074. https://doi.org/10.1093/nar/gkad676.

25. Levy, J.M., Yeh, W.-H., Pendse, N., Davis, J.R., Hennessey, E., Butcher, R., Koblan, L.W., Comander, J., Liu, Q., and Liu, D.R. (2020). Cytosine and adenine base editing of the brain, liver, retina, heart and skeletal muscle of mice via adeno-associated viruses. Nat. Biomed. Eng. *4*, 97–110. https://doi.org/10.1038/s41551-019-0501-5.

26. Su, J., She, K., Song, L., Jin, X., Li, R., Zhao, Q., Xiao, J., Chen, D., Cheng, H., Lu, F., et al. (2023). In vivo base editing rescues photoreceptors in a mouse model of retinitis pigmentosa. Mol. Ther. Nucleic Acids *31*, 596–609. https://doi.org/10.1016/j.omtn.2023.02.011.

27. Suh, S., Choi, E.H., Leinonen, H., Foik, A.T., Newby, G.A., Yeh, W.-H., Dong, Z., Kiser, P.D., Lyon, D.C., Liu, D.R., and Palczewski, K. (2021). Restoration of visual function in adult mice with an inherited retinal disease via adenine base editing. Nat. Biomed. Eng. *5*, 169–178. https://doi.org/10.1038/s41551-020-00632-6.

28. Jang, H.-K., Jo, D.H., Lee, S.-N., Cho, C.S., Jeong, Y.K., Jung, Y., Yu, J., Kim, J.H., Woo, J.-S., and Bae, S. (2021). High-purity production and precise editing of DNA base editing ribonucleoproteins. Sci. Adv. *7*, eabg2661. https://doi.org/10.1126/sciadv.abg2661.

29. Herrera-Barrera, M., Ryals, R.C., Gautam, M., Jozic, A., Landry, M., Korzun, T., Gupta, M., Acosta, C., Stoddard, J., Reynaga, R., et al. (2023). Peptide-guided lipid nanoparticles deliver mRNA to the neural retina of rodents and nonhuman primates. Sci. Adv. *9*, eadd4623. https://doi.org/10.1126/sciadv.add4623.

30. Gautam, M., Jozic, A., Su, G.L.-N., Herrera-Barrera, M., Curtis, A., Arrizabalaga, S., Tschetter, W., Ryals, R.C., and Sahay, G. (2023). Lipid nanoparticles with PEG-variant surface modifications mediate genome editing in the mouse retina. Nat. Commun. *14*, 6468. https://doi.org/10.1038/s41467-023-42189-3.

31. Voltà-Durán, E., Parladé, E., Serna, N., Villaverde, A., Vazquez, E., and Unzueta, U. (2023). Endosomal escape for cell-targeted proteins. Going out after going in. Biotechnol. Adv. *63*, 108103. https://doi.org/10.1016/j.biotechadv.2023.108103.

32. Staahl, B.T., Benekareddy, M., Coulon-Bainier, C., Banfal, A.A., Floor, S.N., Sabo, J.K., Urnes, C., Munares, G.A., Ghosh, A., and Doudna, J.A. (2017). Efficient genome editing in the mouse brain by local delivery of engineered Cas9 ribonucleoprotein complexes. Nat. Biotechnol. *35*, 431–434. https://doi.org/10.1038/nbt.3806.

33. Kallimasioti-Pazi, E.M., Thelakkad Chathoth, K., Taylor, G.C., Meynert, A., Ballinger, T., Kelder, M.J.E., Lalevée, S., Sanli, I., Feil, R., and Wood, A.J. (2018). Heterochromatin delays CRISPR-Cas9 mutagenesis but does not influence the outcome of mutagenic DNA repair. PLoS Biol. *16*, e2005595. https://doi.org/10.1371/journal.pbio.2005595.

34. Horlbeck, M.A., Witkowsky, L.B., Guglielmi, B., Replogle, J.M., Gilbert, L.A., Villalta, J.E., Torigoe, S.E., Tjian, R., and Weissman, J.S. (2016). Nucleosomes impede Cas9

access to DNA *in vivo* and *in vitro*. Elife *5*, e12677. https://doi.org/10.7554/eLife.12677.

35. Isaac, R.S., Jiang, F., Doudna, J.A., Lim, W.A., Narlikar, G.J., and Almeida, R. (2016). Nucleosome breathing and remodeling constrain CRISPR-Cas9 function. Elife *5*, e13450. https://doi.org/10.7554/eLife.13450.

36. Sereda, Y.V., and Bishop, T.C. (2010). Evaluation of elastic rod models with long range interactions for predicting nucleosome stability. J. Biomol. Struct. Dyn. *27*, 867–887. https://doi.org/10.1080/073911010010524948.

37. Stolz, R.C., and Bishop, T.C. (2010). ICM Web: the interactive chromatin modeling web server. Nucleic Acids Res. *38*, W254–W261. https://doi.org/10.1093/nar/gkq496.

38. Ménoret, S., De Cian, A., Tesson, L., Remy, S., Usal, C., Boulé, J.-B., Boix, C., Fontanière, S., Crénéguy, A., Nguyen, T.H., et al. (2015). Homology-directed repair in rodent zygotes using Cas9 and TALEN engineered proteins. Sci. Rep. *5*, 14410. https://doi.org/10.1038/srep14410.

39. Gaudelli, N.M., Lam, D.K., Rees, H.A., Solá-Esteves, N.M., Barrera, L.A., Born, D.A., Edwards, A., Gehrke, J.M., Lee, S.-J., Liquori, A.J., et al. (2020). Directed evolution of adenine base editors with increased activity and therapeutic application. Nat. Biotechnol. *38*, 892–900. https://doi.org/10.1038/s41587-020-0491-6.

40. Huang, T.P., Newby, G.A., and Liu, D.R. (2021). Publisher Correction: Precision genome editing using cytosine and adenine base editors in mammalian cells. Nat. Protoc. *16*, 5740. https://doi.org/10.1038/s41596-021-00525-1.

41. Choi, V.W., Asokan, A., Haberman, R.A., and Samulski, R.J. (2007). Production of recombinant adeno-associated viral vectors. Curr. Protoc. Hum. Genet. *Chapter 12*. Unit 12.9. https://doi.org/10.1002/0471142905.hg1209s53.

42. Aurnhammer, C., Haase, M., Muether, N., Hausl, M., Rauschhuber, C., Huber, I., Nitschko, H., Busch, U., Sing, A., Ehrhardt, A., and Baiker, A. (2012). Universal real-time PCR for the detection and quantification of adeno-associated virus serotype 2-derived inverted terminal repeat sequences. Hum. Gene Ther. Methods *23*, 18–28. https://doi.org/10.1089/hgtb.2011.034.

43. Rames, M., Yu, Y., and Ren, G. (2014). Optimized Negative Staining: a High-throughput Protocol for Examining Small and Asymmetric Protein Structure by Electron Microscopy. JoVE, e51087. https://doi.org/10.3791/51087.

44. Couturier, A., Blot, G., Vignaud, L., Nanteau, C., Slembrouck-Brec, A., Fradot, V., Acar, N., Sahel, J.-A., Tadayoni, R., Thuret, G., et al. (2021). Reproducing diabetic retinopathy features using newly developed human induced-pluripotent stem cell-derived retinal Müller glial cells. Glia *69*, 1679–1693. https://doi.org/10.1002/glia.23983.

45. Love, M.I., Huber, W., and Anders, S. (2014). Moderated estimation of fold change and dispersion for RNA-seq data with DESeq2. Genome Biol. *15*, 550. https://doi.org/10.1186/s13059-014-0550-8.

46. Renier, N., Wu, Z., Simon, D.J., Yang, J., Ariel, P., and Tessier-Lavigne, M. (2014). iDISCO: a simple, rapid method to immunolabel large tissue samples for volume imaging. Cell *159*, 896–910. https://doi.org/10.1016/j.cell.2014.10.010.

47. Vigouroux, R.J., Cesar, Q., Chédotal, A., and Nguyen-Ba-Charvet, K.T. (2020). Revisiting the role of Dcc in visual system development with a novel eye clearing method. Elife *9*, e51275. https://doi.org/10.7554/eLife.51275.